



New UV-initiated lithiated-interpenetrating network gel-polymer electrolytes for lithium-metal batteries

Yuejing Zeng^a, Jin Yang^a, Xiu Shen^{a,**}, Ruiyang Li^a, Zhiqiang Chen^b, Xiao Huang^a, Peng Zhang^{b,***}, Jinbao Zhao^{a,*}

^a State Key Laboratory of Physical Chemistry of Solid Surfaces, Collaborative Innovation Centre of Chemistry for Energy Materials, State-Province Joint Engineering Laboratory of Power Source Technology for New Energy Vehicle, Engineering Research Center of Electrochemical Technology, Ministry of Education, College of Chemistry and Chemical Engineering, Xiamen University, Xiamen, 361005, Fujian, China

^b College of Energy & School of Energy Research, Xiamen University, Xiamen, 361102, Fujian, China

HIGHLIGHTS

- The strength and flexibility eliminates the volume changes of lithium anode.
- The LIPN-GPEs realizes excellent uniform lithium deposition with 4000 h.
- The LIPN-GPEs exhibits better self-supporting nature and high ionic conductivity.
- The LIPN-GPEs reflects fantastic high-voltage resistance characteristic.

ARTICLE INFO

Keywords:

Interface stability
Lithium metal batteries
UV-Irradiation
Thermal stability
Lithiated-interpenetrating network polymer

ABSTRACT

A new lithiated-interpenetrating network gel-polymer electrolytes (LIPN-GPEs) is designed and fabricated by ultraviolet-irradiation radical polymerization. The LIPN-GPEs includes both cross-linked poly (lithiated 2-acrylamido-2-methylpropane sulfonic acid-co-polyethylene glycol acrylate) matrix C-P(AMPSLi-MPEGA) and polyacrylonitrile (C-PAN), which forms the interpenetrating framework. The interpenetrating network ensures the mechanical strength and flexibility that eliminates volume changes of lithium anode during lithium deposition/stripping process. Meanwhile, the LIPN-GPEs with better self-supporting nature and high ionic conductivity (2.5×10^{-3} S/cm) can promote the movement of lithium ion resulting in more uniform distribution, which realizes uniform lithium deposition with stable SEI composition. Therefore, the LIPN-GPEs indicates excellent interfacial stability towards lithium anode. Symmetrical lithium metal cell yields low overpotential of 50 mV over 4000 h at 0.5 mA cm^{-2} . The LIPN-GPEs with optimized ratio exhibits wider electrochemical window (5.06 V vs. Li/Li⁺) at ambient temperature, which also possesses unexceptional thermal stability with decomposition temperature up to 400 °C. Especially, when assembled with high-voltage cathode LiCoO₂ (LCO) and LiNi_{0.5}Co_{0.2}Mn_{0.3}O₂ (NCM523) as coin cells, the LIPN-GPEs reveals cycling performance, reflecting good high-voltage resistance characteristic. This work testifies that LIPN-GPEs through a convenient ultraviolet-irradiation radical polymerization provides a candidate for lithium metal battery, which furnishes application prospects in wearable devices.

1. Introduction

Lithium metal is considered as the most ideal negative material with a high energy density (3860 mAh/g) and low voltage (−3.04 V vs. SHE) [1,2], but its high chemical reaction activity, safety and circulatory

concerns limit its use in liquid electrolytes. Therefore, developing a safer electrolytes system is urgent, in which polymer electrolyte has aroused research interest [3]. Normally, polymer electrolyte can be divided into two classes: solid polymer electrolytes (SPEs) and gel polymer electrolytes (GPEs) [4]. Distinctive from liquid electrolyte, GPEs is safer, while

* Corresponding author.

** Corresponding author.

*** Corresponding author.

E-mail addresses: xiushen@xmu.edu.cn (X. Shen), pengzhang@xmu.edu.cn (P. Zhang), jzbhao@xmu.edu.cn (J. Zhao).

it has higher ionic conductivity than SPEs. Moreover, due to its excellent flexibility and elasticity, it can fully tolerate the huge volume expansion caused by lithium metal during lithium stripping/deposition process, avoiding internal circuit created by the growth of lithium dendrites [5]. As a result, GPEs has been comprehensively studied in recent years [6].

Universally, GPEs consists of polymer host, lithium salts and plasticizers. The functional groups of GPEs can interact with lithium ions, which will facilitate the dissociation of lithium salt thus boosting the ion conductivity. The introduction of plasticizers results in swelling of polymer matrix, bringing it from solid state to GPEs [7]. The polymer matrixes are comprised of polyethylene oxide (PEO) [8], polymethyl methacrylate (PMMA) [9], polyvinylidene fluoride (PVDF) [10,11] and polyacrylonitrile (PAN) [12,13]. Specially, PAN with admirable distinctions of thermal stability and oxidation resistance has been extensively applied into the design of GPEs, which guarantees the mechanical strength of GPEs and inhibits the growth of lithium dendrites [6,14,15]. Though equipped with above superiorities, GPEs still encounters some problems like low ionic conductivity and liquid leakage [16]. Therefore, there is still an urgency to improve the performance of polymer electrolytes.

As for improvement, the leading approaches contain copolymerization, cross-linking, blending and adding active or inert fillers, which aims at ameliorating ionic conductivity and retaining the mechanical strength of polymer framework at the same time [17]. In addition, to successfully impose GPEs into lithium metal batteries, regulating lithium-ion deposition behavior and balancing flexibility and rigidity of polymer framework are another two main measures [18]. The interpenetrating network (IPN) [19–21], a polymer structure that can not only smash the crystalline region of polymer electrolyte but also enhance mechanical strength, chemical performance and thermal stability has been one of crucial structures utilized in the excoitation of GPEs. For example, Ding et al. [22]. Synthesized PEO-based polymer electrolyte mingled with ionic liquid with representative cross-linked network, which demonstrated high ionic conductivity ($>10^{-3}$ S/cm) and powerful mechanical property (6.06 MPa). Lee et al. [23] also designed a cross-linking plastic nitrile polymer electrolyte that can withstand 100 bending cycles with UV-polymerization. As prevent literatures manifest, using such IPN structures can efficiently advance the entanglement of polymer segments to achieve doughtier van der Waals forces between polymer chains and liquid electrolyte [3]. Although the modification of GPEs is relatively perfect, there are still some problems like choice of flexible chain segments and rigid chain segments, the balance between ionic conductivity and the mechanical properties of electrolytes.

In this work, a novel lithiated-interpenetrating network gel polymer electrolytes (LIPN-GPEs) was fabricated through film-casting of mixture including polyethylene glycol acrylate (MPEGA), poly (ethylene glycol) diacrylate (PEGDA) and acrylonitrile (AN) in the presence of lithiated 2-acrylamido-2-methylpropane sulfonic acid (AMPSLi), followed by UV-irradiation polymerization. MPEGA with double bond and PEGDA as cross linker and AMPSLi was first polymerized served as the first component, then AN and PEGDA were added to build an ideal LIPN structure. UV-irradiation is acknowledged as a mature technology based on free radical polymerization, which makes it easier to design and tailor polymer network at a mass production level [24,25]. Flexible oligomer like MPEGA has been famous as flexible segment in polymer host which is also beneficial to improve the interfacial contact, while rigid component like PEGDA is propitious to rigidity of gel polymer electrolyte. As predicted, the prepared LIPN-GPEs displays high ionic conductivity and awesome interfacial compatibility towards anode. It also exhibits super thermal stability and electrochemical performance. Take all aspects into consideration, the obtained LIPN-GPEs indicates its promising application in the next generation of high-energy lithium metal battery.

2. Experimental section

2.1. Synthesis of lithiated-interpenetrating network gel polymer electrolytes

The LIPN-GPEs was acquired by UV-irradiation radical polymerization method. First, 2-acrylamido-2-methylpropane sulfonic acid (AMPS, Aladdin) monomer and stoichiometric molar ratio of lithium carbonate (Li_2CO_3) were mixed uniformly in N, N-dimethylformamide (DMF) by magnetic stirring, subsequently adding Methoxy-polyethylene glycol acrylate (MPEGA, Mn = 480 Sigma-Aldrich) with a molar ratio of AMPS: MPEGA = 2:1 and crosslinker poly(ethylene glycol) diacrylate (PEGDA Mn = 600, 5 wt% of AMPS) and 2-hydroxy-2-methyl propiophenone (HMPP, 0.5 wt% of AMPS) as photo-initiator. Then the precursor solution was cast onto a polyfluorotetraethylene plate with UV-irradiation for 20 min, obtaining the first cross-linking network named as C-AM. Later, the C-AM was cured for another 30 min with different molar ratio of acrylonitrile (AN) (AMPS: AN = 1:2, 1:4, 1:6, 1:8), PEGDA (5 wt% of AN) and HMPP (0.5 wt% of AN), gaining the lithiated-interpenetrating network named as C-AMA. Then they were dried in a vacuum oven at 85 °C for 48 h and transferred into argon-filled glove box, followed by soaking into the liquid electrolyte (1 M LiPF_6 in EC: PC = 1:1 by volume). The eventually received GPEs with different AN ratio was labeled as 2AM4A-GPEs, 2AM8A-GPEs, 2AM12A-GPEs and 2AM16A-GPEs, correspondingly.

2.2. Assembly of the batteries and preparation of electrode

LiCoO_2 (LCO) or $\text{LiNi}_{0.5}\text{Co}_{0.2}\text{Mn}_{0.3}\text{O}_2$ (NCM523, Beijing Easpring Material Technology Co., Ltd) active material together with conductive agent acetylene black (AB) and PVDF with the mass ratio of 8:1:1 were grinded with suitable amount of N-methyl-2-pyrrolidone (NMP) solvent, obtaining uniform NMP-based luxury. Then the luxury was coated on aluminum foil and dried in vacuum oven at 80 °C for 12 h. The loading of the active material is about 1.3 mg cm^{-2} . For liquid electrolyte (LE), it was comprised of 1 M LiPF_6 in EC: DMC = 1:1 vol% (LB-301, Zhangjiagang Guotaihuarong New Chemical Materials Co., Ltd). The as prepared AMA-GPEs was cut into 18.5 mm wafer and was assembled as 2032-type coin cell in the argon glove box. Meanwhile, liquid electrolyte with PE separator (PE-LE) was assembled as 2016-type coin cell.

2.3. Material characterizations

The surface and cross section analysis of dried AMA membrane were exploded by scanning electron microscope (SEM, Zeiss Gemini SEM 500) equipped with energy dispersive X-ray spectroscopy (EDS). The molecular structure information was studied by Fourier transform infrared spectroscopy (FT-IR, Nicolet IS5 spectrometer, Thermo Fisher Scientific Inc) with wave number from 400 to 4000 cm^{-1} and Raman spectroscopy (Horiba, Japan) by employing a Xplora confocal microscopic Raman spectrometer at 532 nm. The differential scanning calorimetry-thermogravimetry (DSC-TG) curves were obtained on a STA 449 Jupiter thermogravimetric analyzer (NETZSCH Company, Germany) with a heating rate of 5 °C min^{-1} in range of 35–700 °C to investigate the thermal stability of electrolyte membrane. X-ray photoelectron spectroscopy (XPS, PHI Quantum 2000) was conducted to analyze the chemical composition of SEI layer. For XPS analysis, the detection limit is about 0.5–0.01 atomic% and the scanning resolution is superior to 0.5 eV (Ag). The in-situ optical microscope pictures were taken by the Optical microscope (Olympus, Japan).

2.4. Electrochemical measurements

The ionic conductivity of AMA-GPEs was measured by electrochemical impedance spectroscopy (EIS) using electrochemical workstation (Solartron, SI-1260, U.K.) with a frequency between 0.1 Hz and

0.1 MHz ranging from 25 °C to 80 °C, in which AMA-GPEs was assembled within two stainless steel (SS) electrodes as a blocking battery. The ionic conductivity (σ , S/cm) of all AMA-GPEs was calculated by following Eq. (1) [26]:

$$\sigma = \frac{L}{s} \times \frac{1}{R_b}$$

where L and S are thickness of AMA-GPEs and area of the stainless steel (SS) respectively, R_b is the bulk resistance tested by EIS.

Electrochemical stability window of AM-GPEs, AMA-GPEs and PE-LE was probed on CHI660E electrochemical workstation (Shanghai Chenhua Instruments Limited) with linear sweep voltammetry (LSV) curve. The asymmetric cell of Li/AMA-GPEs/SS and Li/PE-LE/SS were assembled to measure between 3 and 6 V with a scan rate of 1 mV/s.

To further investigate the electrochemical performance of AMA-GPEs, a battery testing system (NEWARE) was applied to achieve charging and discharging curve at proper voltage. Meanwhile, the interface stability of AMA-GPEs against lithium metal was obtained by assembling Li/Li symmetric cell, which was discharged for 1 h and charged for 1 h at a constant current of 0.5 mA/cm².

3. Results and discussion

The synthesis process of AMA-GPEs is demonstrated in Fig. 1. Firstly, AMPSLi, MPEGAs, PEGDA as cross-linker and photo-initiator HMPP were dissolved in DMF to obtain a homogeneous precursor solution followed by UV-irradiation polymerization to attain the first cross-linked network P(AMPSLi-MPEGAs), which acts as the basic polymer skeleton. The neutralized sulfonate of AMPSLi possesses formidable lyophilic ability and the propyl group have a certain shielding effect on the hydrogen amide group, which is beneficial to further improve the electrochemical stability of electrolyte membrane. Subsequently, a mixed solution of AN and PEGDA in DMF was appended for further UV-illumination to form the interpenetrating framework P(AMPSLi-MPEGAs-AN). PAN-based polymer electrolyte has been reported that $\text{C}\equiv\text{N}$ can strongly interact with Li^+ and $\text{C}=\text{O}$ of carbonate solvent without destructing the mechanical strength [16,27]. In this work, small molecule AN can enter the voids of the first polymerization network to achieve a LIPN structure, thereby promoting the mechanical strength of polymer film and widening the stable electrochemical window at the same time.

Many techniques have been adopted to observe the morphology of the synthesized GPEs. Fig. 2 and Fig. S1 show the surface and cross-

sectional SEM images of dried AMA and AM membrane, respectively. The surface of the dried AMA membrane before plasticizing is relatively flat and smooth without any holes in Fig. 2a and b, making it easy to absorb the electrolyte fully. The homogeneous cross-section image in Fig. 2c and corresponding element distribution Fig. 2d proved that the LIPN structure was successfully formed without hierarchy phenomenon.

FT-IR and Raman were performed to verify the molecular structure of synthesized membrane, as shown in Fig. 3. The monomer AMPS, the first cross-linked network P(AMPSLi-MPEGAs) and LIPN structure P(AMPSLi-MPEGAs-AN) were characterized by FT-IR in Fig. 3a, where the disappearing of $\text{C}=\text{C}$ vibration peak at 1610 cm^{-1} in AMPS made it clear that AMPS has been completely polymerized during UV-irradiation free radical polymerization process. The peak of 1653 cm^{-1} corresponds to the stretching motion of carbonyl group of secondary amide group while the peak at 1546 cm^{-1} ascribes to the plane angular vibration of -CNH , which is labeled as the amide absorption band II. The asymmetrical tensile vibration of the $\text{O}=\text{S}=\text{O}$ is located at peak of 1240 cm^{-1} and peak of 630 cm^{-1} attributes to C-S bond [28]. Extra peak $\text{-C}\equiv\text{N}$ at 2240 cm^{-1} in LIPN structure proved that AN have entered the framework successfully. As shown in Raman spectrum Fig. 3b, after proper plasticization, the peak of $\text{-C}\equiv\text{N}$ moves from (2240 cm^{-1}) to (2250 cm^{-1}), with the trend of decreasing the relative intensity, which demonstrates obvious interaction between $\text{-C}\equiv\text{N}$ and Li^+ [16].

The electrochemical stability window was obtained by assembling Li/AMA-GPEs/SS and Li/PE-LE/SS batteries with linear sweep voltammetry (LSV) at a sweep rate of 1 mV/s. In Fig. 4a, compared to commercially used LE (1 M LiPF_6 in EC: DMC = 1:1 by volume) with approximately 4.24 V (vs. Li/Li^+), both AM-GPEs and AMA-GPEs show obviously larger electrochemical window. Particularly, the measured electrochemical window of 2AM8A-GPEs with optimal ratio is as high as 5.06 V (vs. Li/Li^+), which demonstrates the wonderful high voltage resistance. Such an admirable peculiarity may account for the LIPN structure, which can effectively lock the solvent to prevent side effects from prolonged contact with lithium metal, leading to delaying the decomposition of electrolyte. Importantly, the strong polarity of the polymer membrane skeleton itself greatly promoted the dissociation of Li^+ .

Mechanical strength is another crucial property to estimate the performance of GPEs, which can increasingly influence its electrochemical performance. As shown in Fig. 4b, dried AMA membrane with LIPN structure exhibits great tensile strength with an elongation of 200%, showing an infinite stress value of 0.9 MPa. It manifests that LIPN

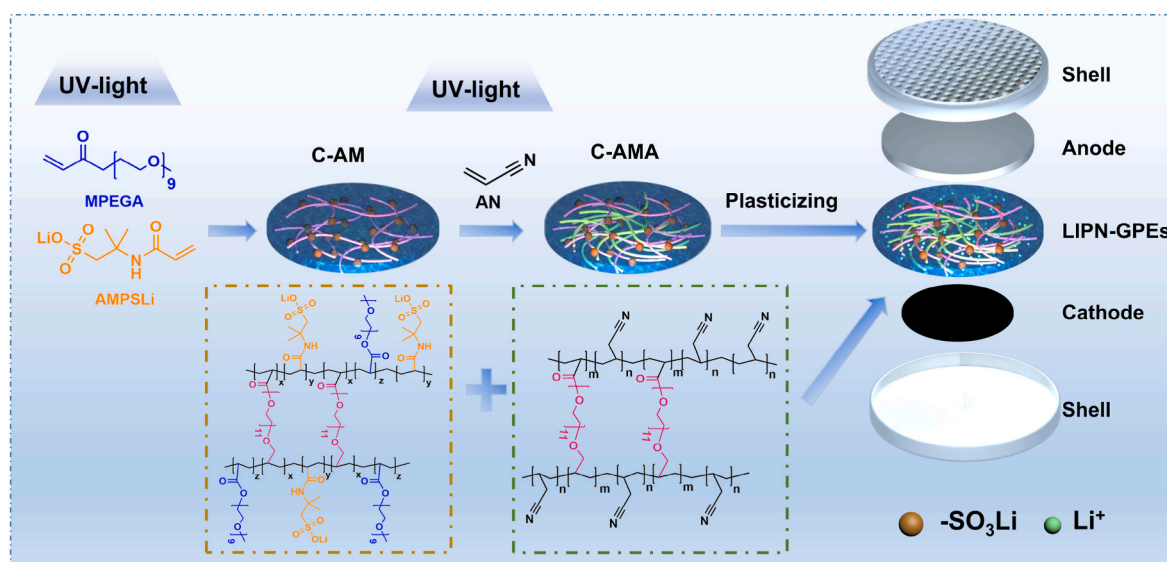


Fig. 1. The illustration of prefabricating lithiated-interpenetrating network gel polymer electrolytes (LIPN-GPEs).

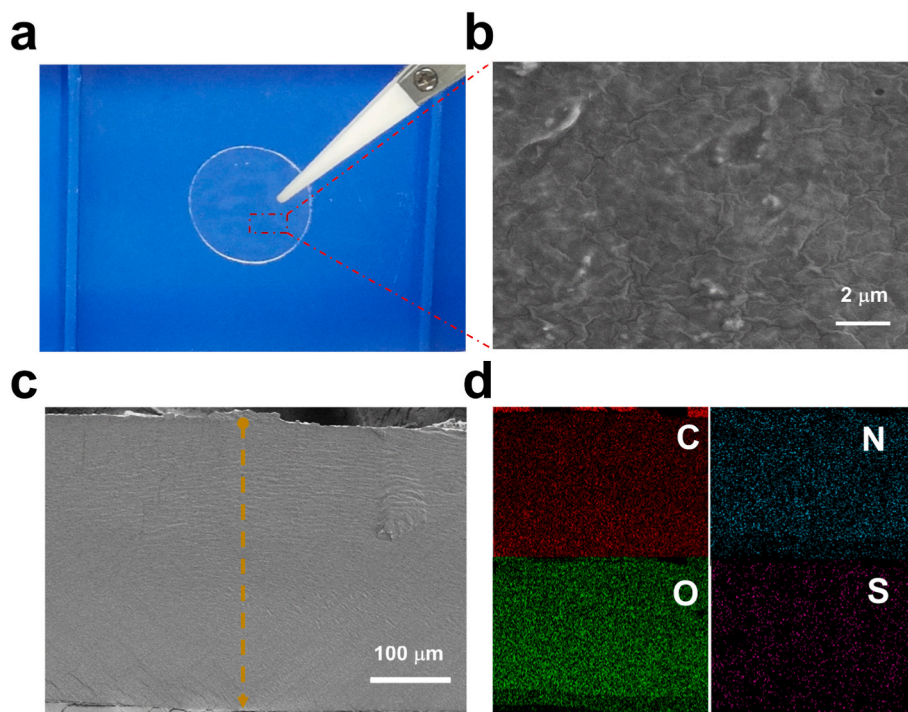


Fig. 2. Photograph (a), surface SEM (b), cross-sectional SEM image (c) and corresponding EDS elemental mapping of C, N, O, S (d) of dried AMA membrane.

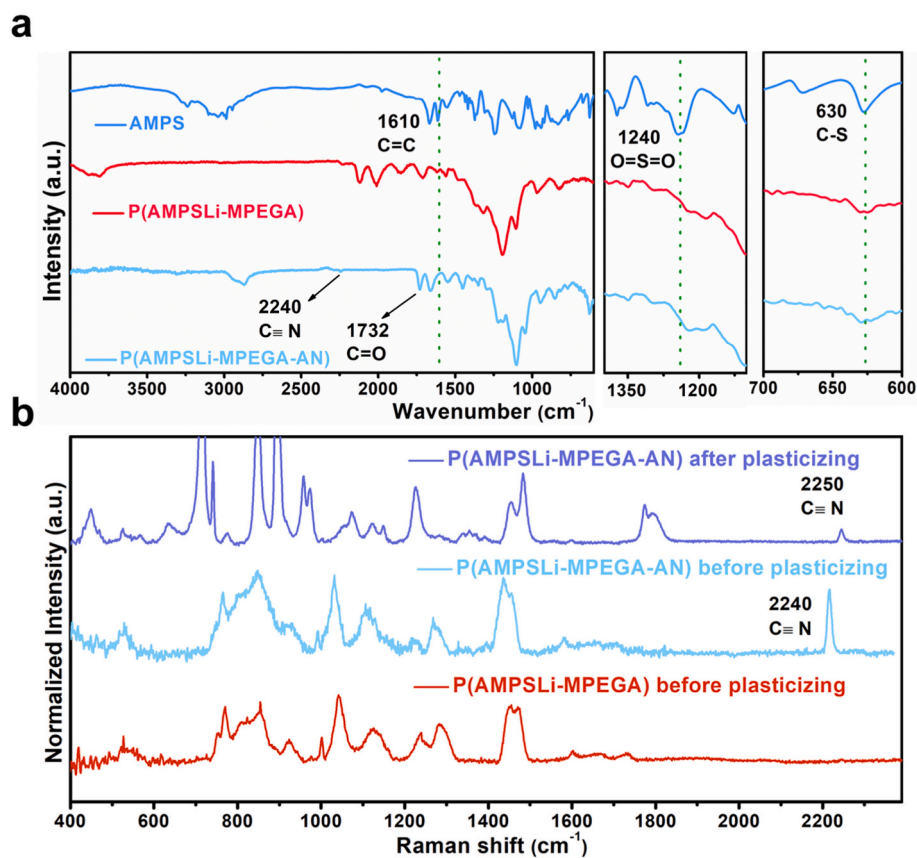


Fig. 3. FT-IR (a) and Raman (b) spectra of AMA-GPEs.

structure can improve the mechanical strength of GPEs, which provides great possibility to utilize in Lithium metal batteries with proper mechanical strength and flexibility.

The relationship between the ionic conductivity and temperature of AMA-GPEs was presented in Fig. 4c, which roughly conformed to Arrhenius equation in the range of 25–80 °C, as follow:

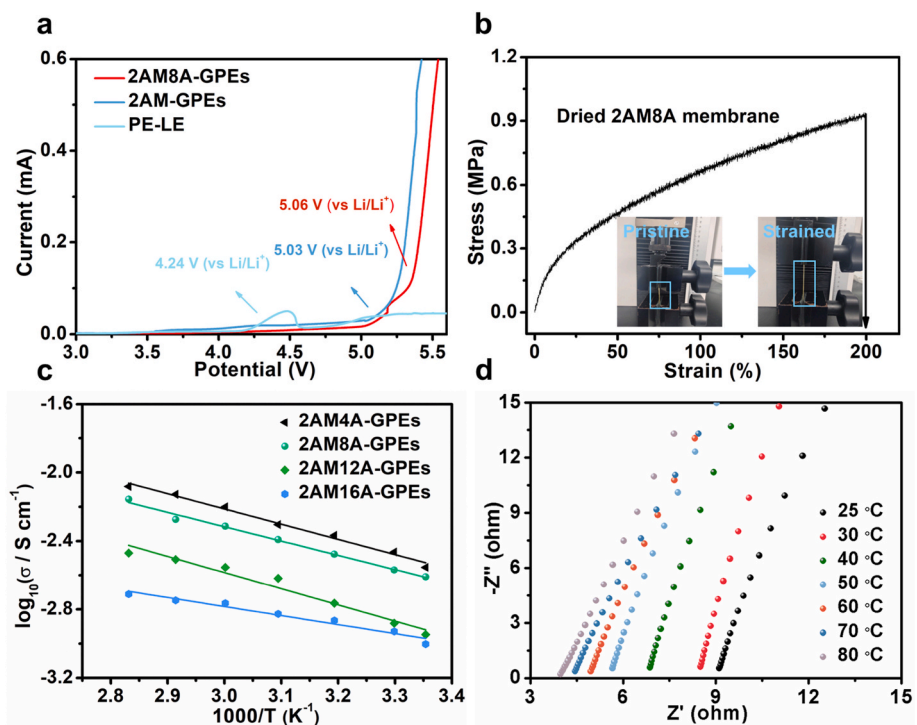


Fig. 4. (a) The LSV plot with Li/GPEs/SS and Li/PE-LE/SS batteries. (b) Strain-stress profile of dried 2AM8A membrane; insides: photos before and after strain. (c) Arrhenius behavior of AMA-GPEs with different ratio. (d) Nyquist plots of SS/2AM8A-GPEs/SS.

$$\lg \sigma = \lg \sigma_0 - \frac{E_a}{2.303RT}$$

Here, σ and σ_0 ascribes to ionic conductivity and pre-factor, E_a corresponds to activation energy, R is the molar gas constant (8.314 J/mol/K). It can be deduced that at the same temperature, the ionic

conductivity of AMA-GPEs gradually decreases with increasing concentration of AN and for a specific proportion of AMA-GPEs, the ionic conductivity will gradually aggrandize with the temperature increasing which fully demonstrates higher temperature can expedite the movement of Li⁺. Specially, 2AM4A-GPEs with lowest proportion of AN possesses the highest ionic conductivity of 2.8×10^{-3} S/cm, while

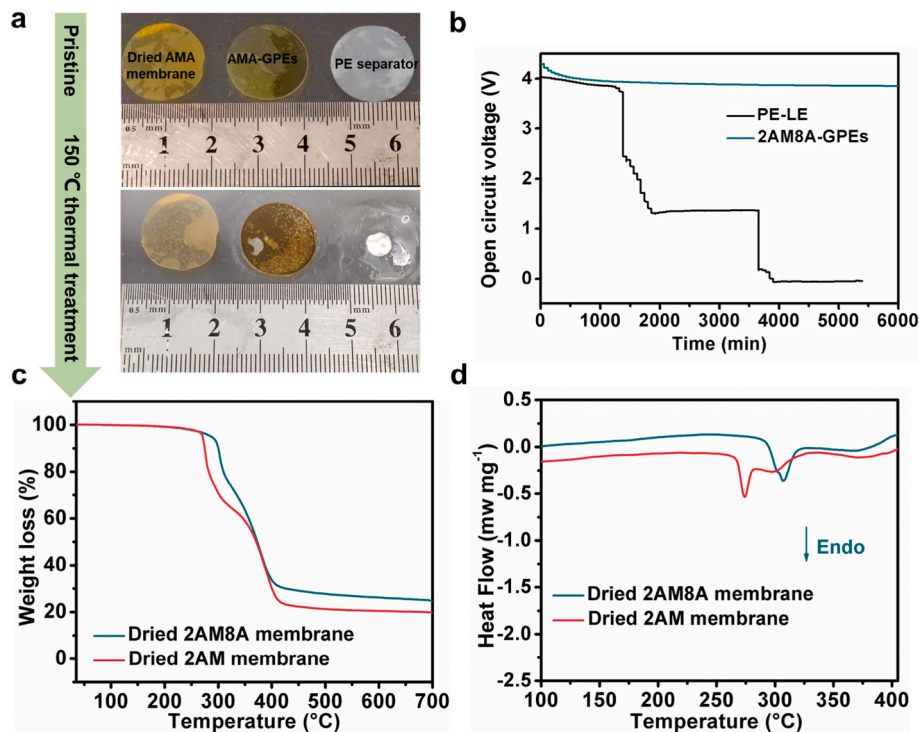


Fig. 5. Optical photos (a) of dried AMA membrane, AMA-GPEs and PE separator respectively after 150 °C thermal treatment for 30 min. OCV curves (b) of 2AM8A-GPEs/LCO and Li/PE-LE/LCO batteries. TG (c) and DSC (d) curves of dried 2AM and 2AM8A membrane.

2AM16A-GPEs with highest concentration of AN exhibit poor ionic conductivity, which declares that the addition of AN optimizes the mechanical strength with sacrifice of ionic conductivity. When adding enough AN, the AMA-GPEs will gradually incarnate the properties of pure PAN-based GPEs. Hence, 2AM8A-GPEs was considered as the optimal ratio. Nyquist plots of 2AM8A-GPEs at different temperature was displayed in Fig. 4d, which was obtained by assembling SS/2AM8A-GPEs/SS battery to test in the frequency ranging from 0.1 Hz to 0.1 MHz. The intersection of the high-frequency region on the real axis represents the bulk resistance (R_b) of the GPEs that can be used for counting the ionic conductivity with high value of 2.5×10^{-3} S/cm at ambient temperature.

The thermal stability of GPEs plays a vital role in the electrochemical performance and safety of the battery. In order to examine the thermal stability of electrolyte membrane, heat-treating at 150 °C for 30 min were conducted for both dried AMA membrane, AMA-GPEs and the PE-LE. As demonstrated in Fig. 5a, after heat-treatment PE separator exhibited obvious thermal shrinkage behavior indicating its poor thermal stability, while the as-prepared membrane can both maintain extremely good morphology before and after immersed in liquid electrolyte, showing its superiority in thermal stability. The open circuit voltage (OCV) curve shown in Fig. 5b with half-cell of Li/AMA-GPEs/LCO demonstrated maintenance of original open circuit potential for a long time after heat-treatment, further verifying its excellent thermal stability. While the half-cell with PE-LE was undergone heat-treatment, its OCV curve appeared a sharp drop which contributed to its thermal shrinkage.

The TG (Fig. 5c) and DSC (Fig. 5d) patterns of dried 2AM and 2AM8A membrane were measured in the temperature range of 35–700 °C at a heating rate of 5 °C/min under argon atmosphere. It can be seen that both dried 2AM and 2AM8A membrane exhibited excellent thermal stability with a decomposition temperature higher than 280 °C. More significantly, 2AM8A membrane with LIPN structure exhibited better performance, whose onset decomposition temperature of 300 °C and 380 °C corresponded to the degradation of PEG segments [29] and $-\text{SO}_2$

[26,30] respectively. A maximum decomposition temperature of 400 °C sufficiently showed excellent thermal stability, which can fully meet the actual battery requirements.

Symmetrical lithium metal batteries were assembled to obtain the galvanostatic polarization curve, which can be used to reflect the dynamics interface stability between the GPEs and lithium metal. Fig. 6a was the cycling curve when using AMA-GPEs and commercial LE (1 M LiPF_6 in EC: DMC = 1:1 by volume) respectively, in which the current density was 0.5 mA/cm^2 , 0.5 mAh cm^{-2} . When commercial LE was employed, its initial polarization voltage was about 100 mV and gradually decreased followed by increasing sustainably, finally reaching a high voltage of 150 mV after cycling for 1000 h. While using AMA-GPEs, the original polarization potential is approximate 50 mV and in the initial activation process the polarization voltage appears a small decrease and then almost keeps stable for a long time. After a long cycling, it gradually occurs a negligible decreasing trend for the continuous dissociation of lithium ions in AMPSLi matrix, which fully indicated excellent interface stability between AMA-GPEs and lithium metal. Such an excellent result may benefit from the moderate flexibility of AMA-GPEs allowing it to adhere to the lithium metal and its sufficient mechanical strength can effectively inhibit the growth of lithium dendrites. Meanwhile, since the AMA-GPEs has better liquid adsorption capacity, it can drastically promote the movement of lithium ions between lithium metal and AMA-GPEs. Thus, more uniform distribution of Li^+ near the lithium anode resulting in more uniform lithium deposition, leading to a more stable SEI composition.

Fig. 6b and c were the mechanism of lithium deposition/stripping process when using commercial LE and AMA-GPEs, which can be deduced from the previous analysis and discussion. Under optical microscope, it can be easily observed that after 4 h of lithium deposition at a current density of 0.5 mA/cm^2 , lithium dendrites were obviously grown when using commercial LE in Fig. 6d, while a relatively flat lithium deposition layer can be obtained in Fig. 6e using 2AM8A-GPEs. The result further demonstrated the excellent interface stability between the obtained 2AM8A-GPEs and lithium metal, which also confirmed its

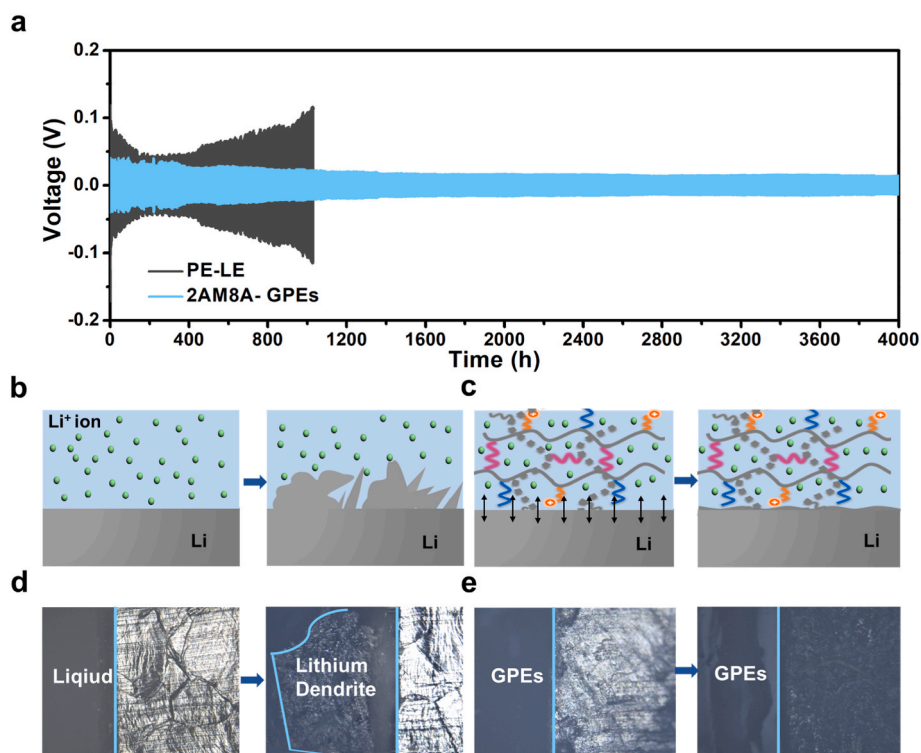


Fig. 6. Curves of Li/2AM8A-GPEs/Li and Li/PE-LE/Li at room temperature with 0.5 mA cm^{-2} , 0.5 mAh cm^{-2} (a). Schematic diagram of mechanism for Li deposition/stripping with LE (b) and AMA-GPEs (c). Optical microscope pictures of LE (d) and AMA-GPEs (e) before and after Li deposition for 4 h with 0.5 mA cm^{-2} .

excellent cycling performance of symmetrical lithium metal cell.

In order to verify the cycling performance and high-voltage resistance of the AMA-GPEs in the lithium metal battery, the Li/AMA-GPEs/LCO half-cell was assembled, while Li/PE-LE/LCO half-battery was assembled at the same time. Fig. 7a showed the variation of coulomb efficiency and discharge capacity with the number of charge and discharge cycles respectively, where the half-cells were charged and discharged at 0.2 C between 3.0 and 4.4 V. The first charge/discharge profile of Li/AMA-GPEs/LCO half-cell was showed in Fig. S2. During the entire cycling process, the coulombic efficiency of the two half-cells was both preserved at about 100%, though the half-cell using commercial LE showed a low-capacity retention rate of 50% extremely less than that of 78% in AMA-GPEs. Furthermore, Li/AMA-GPEs/NCM523 half-battery was also performed at 0.2 C between 3.0 and 4.3 V, whose excellent cycling curve was presented in Fig. S3 and Fig. S4. This fully showed that the synthesized AMA-GPEs can exhibit excellent cycling performance in combination with high-voltage cathode materials.

Excellent cycling performance of AMA-GPEs was propitious to stable SEI composition. The SEI chemical composition of the Li/PE-LE/LCO and Li/AMA-GPEs/LCO half-cells on the lithium metal electrode (after 10 cycles of charging and discharging at 0.2 C) obtained by applying X-ray photoelectron spectroscopy (XPS) technology were shown in Fig. 7b–e and Fig. 7f–i, correspondingly. The peaks of C 1s, N 1s, O 1s and S 2p were situated at 284, 400, 532 and 160 eV, respectively. In Fig. 7b–e, the C 1s spectrum showed C–O (287.9 eV), C=O (284.5 eV) and CO₃²⁻ (289.3 eV) groups derived from the decomposition of solvent molecules in the LE, which were the main components of the SEI layer

on the electrode such as lithium carbide, lithium alkyl carbonate or lithium carbonate [31]. Correspondingly, two strong peaks C–O (532.8 eV) and C=O (531.0 eV) can be observed on the corresponding O 1s spectrum. The content of inorganic chemical composition is obviously excess to organic chemical composition, indicating the brittle SEI layer on lithium anode in LE-PE system.

The SEI chemical composition of Li/AMA-GPEs/LCO half-cell on the lithium metal electrode exhibits differently. In Fig. 7f–i, C–O (286.3 eV), C=O (288.9 eV) and CO₃²⁻ (290.7 eV) groups in C 1s spectrum can be observed, which showed that the SEI component had some conventional main components. Compared to LE-PE system, its SEI component includes more organic chemical composition than inorganic chemical composition, revealing an elastic SEI layer. Besides, in N 1s spectrum, there exists two strong signal peaks of Li₃N (399.4 eV) and LiN_xO_y (400.3 eV). Li₃N was treated as a lithium superionic conductor [32], which can greatly improve the lithium-ion conductivity on SEI layer and contribute to inhibit the growth of lithium dendrites [33]. As far as S 2p spectrum was concerned, the peaks of 168.2 eV, 163.3 eV and 161.0 eV corresponds to R–SO₃, S²⁻ and Li₂S [34,35], respectively. Based on the above analysis, when using AMA-GPEs in half-cells, the SEI components were more diversified to form a more stable SEI, which was conducive to the long-cycle operation of the battery. Among them, the inorganic components Li₃N and Li₂S played an important role in the rapid conduction of lithium ions, which was essential to improve the cycle performance of the battery. The formation of such a stable SEI components may be derived from the LIPN structure of AMA-GPEs, which had a stronger liquid absorption capacity and thus can effectively inhibit the

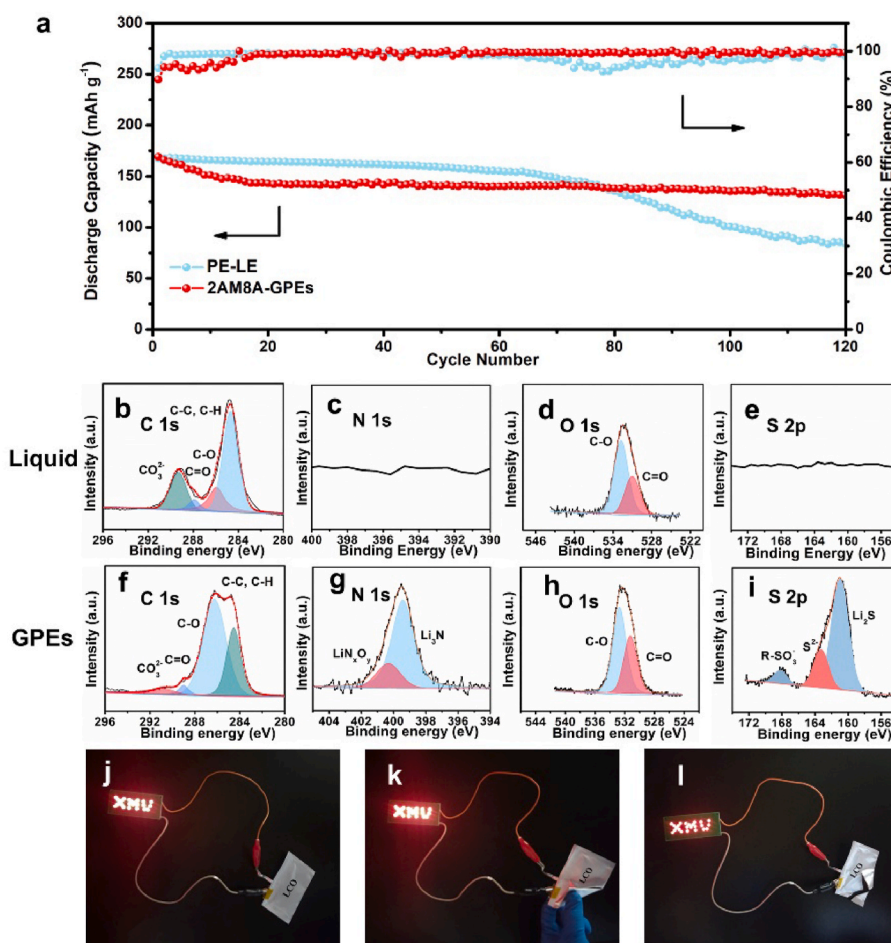


Fig. 7. Cycling performance (a) of Li/2AM8A-GPEs/LCO and Li/PE-LE/LCO coin cells between 3.0 and 4.4 V at 0.2 C. XPS analysis on Li anode of Li||LCO battery of C 1s, N 1s, O 1s and S 2p spectra of SEI layer after cycling for LE (b–e) and 2AM8A-GPEs (f–i) correspondingly. Photograph of LED device lighted by AMA-GPEs pouch cell (j) pristine state, (k) folding, (l) cutting.

decomposition of solvent molecules. This fully demonstrated the effectiveness and reliability of the strategy of LIPN structure used in this study.

The soft pack battery based on AMA-GPEs showed excellent flexibility, which may be related to the as-designed LIPN structure. As shown in the Fig. 7j-l, the assembled pouch battery can successfully light up the LED device and can continue to power without attenuation after folding and cutting. Such excellent performance fully showed that the prepared flexible battery can be applied to wearable devices.

4. Conclusions

In this work, a new lithiated-interpenetrating network gel-polymer electrolytes (LIPN-GPEs) was obtained by means of radical polymerization under ultraviolet light. The interpenetrating network ensures the mechanical strength with better self-supporting nature and endows it with higher ionic conductivity and flexibility. Meanwhile, the LIPN-GPEs can also promote the movement of Li^+ resulting in more uniform distribution, realizing excellent uniform lithium deposition with stable SEI composition. Therefore, the LIPN-GPEs indicates excellent interfacial stability towards lithium anode. Symmetrical lithium metal cell yields low overpotential of 50 mV over 4000 h at 0.5 mA cm^{-2} . The LIPN-GPEs with optimized ratio exhibits high ionic conductivity (2.5×10^{-3} S/cm) and wider electrochemical window (5.06 V vs. Li/Li^+) at ambient temperature, which also possesses unexceptional thermal stability with decomposition temperature up to 400 °C. Additionally, when assembled with high-voltage cathode LiCoO_2 (LCO) and $\text{LiNi}_{0.5}\text{Co}_{0.2}\text{Mn}_{0.3}\text{O}_2$ (NCM523) as coin cells, the LIPN-GPEs reveals cycling performance, reflecting good high-voltage resistance characteristic. In summary, the synthesized LIPN-GPEs will be a promising option for lithium metal batteries in future with convenient fabrication of UV- irradiation radical polymerization which can also be widely used in wearable devices.

CRedit authorship contribution statement

Yuejing Zeng: Conceptualization, Methodology, Writing – original draft, preparation. **Jin Yang:** Data curation, Writing – original draft, preparation. **Xiu Shen:** Data curation, Writing – review & editing. **Ruiyang Li:** Visualization. **Zhiqiang Chen:** Investigation. **Xiao Huang:** Investigation. **Peng Zhang:** Supervision, Writing – review & editing. **Jinbao Zhao:** Project administration, Funding acquisition.

Declaration of competing interest

The authors declare that they have no known competing financial interests or personal relationships that could have appeared to influence the work reported in this paper.

Acknowledgments

This work was financially supported by the National Natural Science Foundation of China (21875195, 22021001), Fundamental Research Funds for the Central Universities (20720190040), National Fund for Talent Training in Basic Science (J1310024) and The Key Project of Science and Technology of Xiamen (3502Z20201013). Thanks Kah Kee Innovation Laboratory for SEM measurement.

Appendix A. Supplementary data

Supplementary data to this article can be found online at <https://doi.org/10.1016/j.jpowsour.2022.231681>.

References

- [1] J. Liu, H. Ma, Z. Wen, H. Li, J. Yang, N. Pei, P. Zhang, J. Zhao, J. Energy Chem. 64 (2022) 354–363.
- [2] Y. Zhang, J. Dong, C. Tan, S. Huo, J. Wang, Y. He, Y. Wang, J. Electrochem. 27 (2021) 108–117.
- [3] V. Chaudoy, F. Ghamouss, E. Luais, F. Tran-Van, Ind. Eng. Chem. Res. 55 (2016) 9925–9933.
- [4] H. Li, Z. Xu, J. Yang, J. Wang, S.-i. Hirano, Sustain. Energy Fuels 4 (2020) 5469–5487.
- [5] X. Zhao, C.-a. Tao, Y. Li, X. Chen, J. Wang, H. Gong, Ionics 26 (2020) 4299–4309.
- [6] X. Zhang, S. Zhao, W. Fan, J. Wang, C. Li, Electrochim. Acta 301 (2019) 304–311.
- [7] D. Zhou, D. Shanmukaraj, A. Tkacheva, M. Armand, G. Wang, Inside Chem. 5 (2019) 2326–2352.
- [8] J. Fu, Q. Lu, D. Shang, L. Chen, Y. Jiang, Y. Xu, J. Yin, X. Dong, W. Deng, S. Yuan, J. Mater. Sci. 53 (2018) 8420–8435.
- [9] Y. Zhang, Y.-Z. Song, J.-J. Yuan, X. Yin, C.-C. Sun, B.-K. Zhu, J. Appl. Polym. Sci. 135 (2018) 46423.
- [10] Y. Xia, Y.F. Liang, D. Xie, X.L. Wang, S.Z. Zhang, X.H. Xia, C.D. Gu, J.P. Tu, Chem. Eng. J. 358 (2019) 1047–1053.
- [11] S.K. Singh, H. Gupta, L. Balo, Shalu, V.K. Singh, A.K. Tripathi, Y.L. Verma, R. K. Singh, Ionics 24 (2018) 1895–1906.
- [12] C.F. He, J.Q. Liu, J.Q. Cui, J. Li, X.F. Wu, Solid State Ionics 315 (2018) 102–110.
- [13] F. Pignatelli, M. Romero, R. Faccio, L. Fernández-Werner, A.W. Mombrú, J. Phys. Chem. C 122 (2018) 1492–1499.
- [14] W. Fan, X. Zhang, C. Li, S. Zhao, J. Wang, ACS Appl. Energy Mater. 2 (2019) 4513–4520.
- [15] C. Fu, Y. Ma, S. Lou, C. Cui, L. Xiang, W. Zhao, P. Zuo, J. Wang, Y. Gao, G. Yin, J. Mater. Chem. 8 (2020) 2066–2073.
- [16] S.-H. Wang, P.-L. Kuo, C.-T. Hsieh, H. Teng, ACS Appl. Mater. Interfaces 6 (2014) 19360–19370.
- [17] L. Fan, H. He, C. Nan, Nat. Rev. Mater. 6 (2021) 1003–1019.
- [18] J. Shi, Y.F. Yang, H.X. Shao, J. Membr. Sci. 547 (2018) 1–10.
- [19] X. Shen, L. Peng, R. Li, H. Li, X. Wang, B. Huang, D. Wu, P. Zhang, J. Zhao, Chemelectrochem 6 (2019) 4483–4490.
- [20] M. Liu, S. Zhang, G. Li, C. Wang, B. Li, M. Li, Y. Wang, H. Ming, Y. Wen, J. Qiu, J. Chen, P. Zhao, J. Power Sources 484 (2021) 229235.
- [21] C. Fu, X. Zhang, C. Cui, X. Zhang, S. Lou, Y. Ma, H. Huo, Y. Gao, P. Zuo, G. Yin, Chem. Eng. J. 432 (2022).
- [22] Y.H. Li, Z.J. Sun, L. Shi, S.Y. Lu, Z.H. Sun, Y.C. Shi, H. Wu, Y.F. Zhang, S.J. Ding, Chem. Eng. J. 375 (2019) 121925.
- [23] H.-J. Ha, E.-H. Kil, Y.H. Kwon, J.Y. Kim, C.K. Lee, S.-Y. Lee, Energy Environ. Sci. 5 (2012) 6491–6499.
- [24] E.-H. Lee, J.-H. Park, J.-M. Kim, S.-Y. Lee, Electrochim. Acta 104 (2013) 249–254.
- [25] C. Fu, Y. Ma, P. Zuo, W. Zhao, W. Tang, G. Yin, J. Wang, Y. Gao, J. Power Sources (2021) 496.
- [26] X. Shen, H. Hua, H. Li, R. Li, T. Hu, D. Wu, P. Zhang, J. Zhao, Polymer 201 (2020) 122568.
- [27] B. Wu, Q. Liu, D. Mu, Y. Ren, Y. Li, L. Wang, H. Xu, F. Wu, J. Phys. Chem. C 118 (2014) 28369–28376.
- [28] J. Cong, X. Shen, Z. Wen, X. Wang, L. Peng, J. Zeng, J. Zhao, Energy Storage Mater. 35 (2021) 586–594.
- [29] L.N. Wang, X.C. Zhan, Z.G. Zhang, K.L. Zhang, J. Alloys Compd. 456 (2008) 461–465.
- [30] W.-W. Cui, D.-Y. Tang, J. Appl. Polym. Sci. 126 (2012) 510–518.
- [31] J. Bae, Y. Qian, Y. Li, X. Zhou, J.B. Goodenough, G. Yu, Energy Environ. Sci. 12 (2019) 3319–3327.
- [32] S. Liu, X. Ji, N. Piao, J. Chen, N. Eidson, J. Xu, P. Wang, L. Chen, J. Zhang, T. Deng, S. Hou, T. Jin, H. Wan, J. Li, J. Tu, C. Wang, Angew. Chem., Int. Ed. Engl. 60 (2021) 3661–3671.
- [33] N.-W. Li, Y.-X. Yin, J.-Y. Li, C.-H. Zhang, Y.-G. Guo, Adv. Sci. 4 (2017) 1600400.
- [34] R. Grissa, V. Fernandez, N. Fairley, J. Hamon, N. Stephant, J. Rolland, R. Bouchet, M. Lecuyer, M. Deschamps, D. Guyomard, P. Moreau, ACS Appl. Energy Mater. 1 (2018) 5694–5702.
- [35] J.E. Morales-Ugarte, A. Benayad, C.C. Santini, R. Bouchet, ACS Appl. Mater. Interfaces 11 (2019) 21955–21964.